

# The Role of Sintering Additives on Synthesis of High Performance Ceramic- Matrix Composites (Cmcs) by Volume Combustion in The $\text{TiO}_2\text{-Al-C}$ System: Structural and Mechanical Properties

Badis Bendjemil<sup>1,2\*</sup>, Mohamed Mouyane<sup>3</sup>, Jacques G. Noudem<sup>4</sup>, Jérôme Bernard<sup>3</sup>, Jean Michel Reboul<sup>3</sup>, Yannick Guel<sup>2</sup> and David Houivet<sup>3</sup>

<sup>1</sup>DGM/FST/UG-Université 08 Mai 1945 Guelma, avenue 19 Mai 1956, CS 401, 24000 Guelma, Algeria

<sup>2</sup>LASEA/DC/FS/UBMA-University of Badji-Mokhtar Annaba, CS 12, 23000 Annaba, Algeria

<sup>3</sup>LUSAC, EA 4253, 60 rue Max Pol Fouchet, CS 20082, Université de Caen Basse-Normandie (UCBN), 50130 Cherbourg-Octeville, France

<sup>4</sup>ENSICAEN, 6, Boulevard Maréchal Juin, CS 45053 14050 Caen Cedex 04, France

## \*Corresponding author

Badis Bendjemil, DGM/FST/UG-Université 08 Mai 1945 Guelma, avenue 19 Mai 1956, CS 401, 24000 Guelma, Algeria, Tel:00213674301959; E-mail:Badis23@gmail.com

Submitted: 16 Aug 2019; Accepted: 17 Sep 2019; Published: 23 Dec 2019

## Abstract

The purpose of this work is to decrease or eliminate porosities in ETE-VC products with sintering additives. The Ti-C system has been synthesized for its advantages for refractory, abrasive and structural applications. We attempted to density TiC by using iron addition; this metal is introduced through a secondary reaction  $3\text{TiO}_3 + \text{Al}$ . This mixture reacts exothermically  $\Delta H_{298} = -1072.7 \text{ kJ}$  and the heat is released according to by Fe addition  $3\text{TiO}_3 + 4\text{Al} + 3\text{C} + x\text{Fe} \rightarrow 3\text{TiC} + 2\text{Al}_2\text{O}_3 + x\text{Fe}$ . X-ray diffraction analysis indicated that intermetallic Fe<sub>3</sub>Al, TiC and Al<sub>2</sub>O<sub>3</sub> are the main phases formed in the reinforced high performance ceramic-matrix composites and the additions of Fe decreased the lattice parameter of TiC. Field emission scanning electron microscopy examinations showed that the addition of Fe decreased TiC particle size and changed their growth controlling mechanism. Also, Raman spectroscopy analysis showed that at higher Fe contents, oxygen dissolved in the TiC crystal structure leading to the formation of titanium oxy-carbide with lower lattice parameter and residual un-reacted carbon in the products. The adiabatic temperatures for the reactions containing % Fe estimated using the thermodynamic data. Thus, doping method is finally used to fabricate materials by ETE-VC method (volume combustion method) for industrial applications.

**Keywords:** Thermal Explosion Reaction,  $\text{TiO}_2\text{-Al-C-Fe}$  System, Raman Analysis: TiC Growth Mechanism High Performance Ceramics Matrix Composite

## Introduction

The particle reinforced metal-matrix composites are a group of materials which can be used in wear and corrosion resistance applications because of their low costs, the ease of fabrication, high stiffness and elastic modulus and isotropic properties [1,2]. Despite of the higher density of iron base composites, their lower output costs and more isotropic properties make these materials attractive for many applications. The types of reinforcements, their compatibility with the matrix and their volume fraction have considerable effects on the properties of these composites [3]. Among all ceramic reinforcing particles, titanium carbide (TiC) due to its outstanding properties including high melting point (3250°C), high hardness (2890–3200 HV), low density (4.93 g/cm<sup>3</sup>), high

elastic modulus (269 GPa), excellent corrosion resistance and good thermodynamic stability with the Fe melt is a proper candidate for fabricating Fe based composites [1,4,5]. The electrothermal explosion process is a low cost and quick process for the production of different ceramics, ceramic matrix and metal matrix composites [6-9]. This procedure usually is divided into two different categories called volume combustion synthesis (VC). During VC, samples are heated uniformly to the reaction initiation temperature. Then, the reaction starts in all parts of the sample simultaneously. Once the reaction starts, the heat liberated provides the necessary heat for its propagation along the entire sample. Lower costs and simplicity are the advantages of ETE-VC over volume combustion [8]. Fabrication of TiC and composites containing this compound by the ETE-VC process was the main topic of many researches [6-8, 10-19]. Among different combustion reactions, reduction of titanium oxide ( $\text{TiO}_2$ ) with aluminum in the presence of carbon is an exothermic reaction which goes to the formation of a composite which consists of TiC

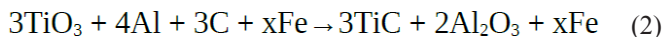
and aluminum oxide (Al<sub>2</sub>O<sub>3</sub>). This reaction, which usually is called aluminothermic reduction of TiO<sub>2</sub>, is as follows:



If a metallic element is added to this reaction and it only acts as a diluents agent, different metal matrix composites consisting of TiC and Al<sub>2</sub>O<sub>3</sub> particles as reinforcements can be created. Xia and others produced Al–TiC–Al<sub>2</sub>O<sub>3</sub> composite by adding excess Al to reaction 1 [18]. They showed that the critical molar ratio of excess aluminum, which the combustion reaction can self- sustain with a preheat temperature of 400–500 K is 7.66 mol. Zhu and co-workers [18] controlled C/TiO<sub>2</sub> molar ratio to fabricate different composites including Al<sub>3</sub>Ti–Al<sub>2</sub>O<sub>3</sub>, Al<sub>3</sub>Ti–Al<sub>2</sub>O<sub>3</sub>–TiC and Al<sub>2</sub>O<sub>3</sub>–TiC.

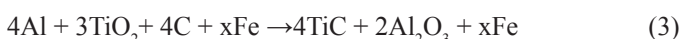
Recently some attempts have been performed for fabricating Fe–TiC–Al<sub>2</sub>O<sub>3</sub> composite from ilmenite concentrations by carbo-aluminothermic reduction process [3,20]. But, there is no report on the effect of Fe additions to the aluminothermic reduction of TiO<sub>2</sub> in the open literature. So, in the present work we added various amounts of Fe to reaction 1 and investigated the effect of this parameter on microstructure and phases that are formed after ETE-VC.

The aim of the present study was to investigate the outcome of iron addition on ETE-VC characteristics and phases that formed during volume combustion synthesis of the TiO<sub>2</sub>-Al-C system. The considered reaction is as follows:



The precursors used in this work are were titanium oxide (TiO<sub>2</sub> Anatas, purity higher than 99.5 %, 45µm), activated carbon (Merck, 102184), fine aluminum powder (Rankem, A2265) and ironm, activated carbon (Merck, 102184), fine aluminum powder (Rankem, A2265) and iron powder (purity higher than 99 wt. % ≤ 100 µm), activated carbon (Merck, 102184), fine aluminum powder (Rankem, A2265) and ironm).

The powders are weighted corresponding to the following expected reactions respectively:



According to the above calculations, the amounts of Fe added to the reaction were between 0 and 60 wt. % before ETE-VC.

To obtain homogenized and fine powder mixtures, the powder mixtures were ball-milled at a high speed of 200 RPM for 30 min by using WC balls (diameter: 3 mm) to powder ratio of 10:1 using balls to produce a homogenous mixture.

Then, the mixtures were pressed in a tool cooper die and cylindrical compacts with 10 mm diameter, and 20 mm of thickness and 60% of theoretical density was prepared.

The ETE-VC process was performed in argon atmosphere with purity higher than 99 wt. %. Fig. 1 shows a schematic representation

of ETE-VC chamber. Prior to ETE-VC, the argon gas was purged into the chamber with a flow rate of 6 l/min for 4–6 min to ensure that the air in the container is minimized. Also, during synthesis and cooling of samples, the gas flow rate was kept constant at 4 l/min. The necessary heat for ignition of the reaction was provided by passing a 10000 Amper electrical current through two cooper electrode with 20 mm in diameter. The green compact is placed inbetween.

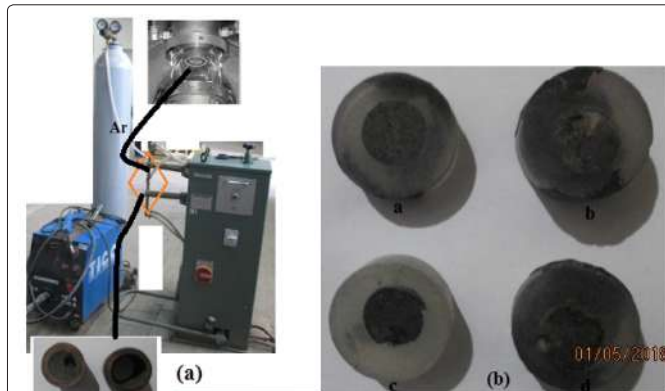


**Figure 1:** Schematic representation of ETE-VC chamber and produced samples (b)

To characterize the reaction products, X-ray diffraction (XRD) analysis was performed with Cu Kα radiation. Raman spectroscopy was performed using a dispersive Raman microscope with a confocal depth resolution of 2µm), activated carbon (Merck, 102184), fine aluminum powder (Rankem, A2265) and ironm, spectral resolution of b 3cm<sup>-1</sup> and spectral range between 160 and 3500 cm<sup>-1</sup> by 785 nm laser. Spectra were taken from different points of the samples to determine the homogeneity and to identify various compounds formed in the samples. Also, microstructures of the products were studied using a field emission scanning electron microscope (FESEM, Cambridge S360).

The **wear resistance** and the **friction coefficient** will be performed in the near future. The microhardness (**H**), the elastic modulus (**E**) and the toughness (**K<sub>IC</sub>**) of the fabricated samples were measured under ambient conditions using the instrumented **Vickers** indentation method (ZwickRoell, ZHU 2.5 apparatus).

The impression diagonal (**2a**) was measured, and the hardness values were calculated according to the following relation:

$$H_v = (1.8544.P)/(2a)^2 \dots \dots \dots (3)$$

The fracture toughness was also calculated by indentation fracture (IF) method according to the equation:

$$K_{IC} = 0.16H_v a^{1/2} (c/a)^{-3/2} \quad (4)$$

Where **H<sub>v</sub>** was the **Vickers** hardness, **a** was the half-length of the indentation diagonal and **c** was the half-length of the median crack generated by indentation. Generally, the fracture toughness measured by **IF** method were fluctuating values with relatively large deviations due to the phase distribution and measurement errors of calculation. Thus a linear regression model was applied to get a reliable value of indentation fracture toughness [21].

To obtain the values of **A**, **B** and **R**<sup>2</sup>, a series of indentation loads (**10 N, 50 N, 100 N, 300, 500N**) were applied to get the relations of **P** and **c**<sup>3/2</sup>

Where **P** is the indentation load. Through the combination of Eqs. (5) and (6), a linear relation between **P** and **c**<sup>3/2</sup> was obtained:

$$P = Ac^{3/2} + B \quad (A = K_{IC}/0.075) \quad (5)$$

## Results and discussion

### Thermodynamic calculations

The aluminothermic reaction of titanium oxide in the presence of iron considered in the present work is as follows:



According to thermodynamic data, in the absence of Fe, the enthalpy of this reaction is extremely negative and hence it is considerably exothermic, but the addition of iron decreases the heat released from this reaction. So, before experimental investigations, thermodynamic calculations were performed to determine the range that iron can be added to reaction2 (x) and still it will heated. In exothermic reactions, if the conditions are assumed to be adiabatic, the heat liberated from the reaction can increase the final temperature of the wares. The highest temperature that a reaction system can reach is adiabatic temperature (**T<sub>ad</sub>**) and can be calculated using the following formula [8]:

$$\Delta H = \int_{298}^{T_{tr}} nC_p(\text{products})dT + n\Delta H_{tr} + \int_{T_{tr}}^{T_{ad}} nC_p(\text{products})dT \quad (6)$$

Is the difference between the formation of molar enthalpy of the products and raw materials at 298 K, n is the mole of each product and C<sub>p</sub> is the molar heat capacity. If there is any phase change in products during heating, it should be considered in the calculations. So, in the previous formula, T<sub>tr</sub> is the transformation temperature and ΔH<sub>tr</sub> is the molar enthalpy of transformation. Also, if a material is added to the reaction as diluents, its heat capacity should be added to the product's heat capacity. Combustion wave is dependent on the heat generation by the reaction and heat dissipation to the surrounding area and remaining reactants. The low adiabatic temperature of a reaction indicates that the heat generated by this reaction is low and therefore this reaction cannot propagate in a stable mode [9]. According to the experimental criterion of Merzhanov, in an exothermic reaction if the calculated adiabatic temperature is higher than 1800 K, it can be volume combustion and the process is (ETE) [9,10]. The effect of Fe additions on the adiabatic temperature of reaction2 is shown in Fig. 1. Also, thermodynamic data used for calculating the adiabatic temperature is presented in Table 1. According to Fig. 2, adiabatic temperature of the aluminothermic reaction of titanium oxide is 2371 K and addition of iron decreases it with a non-uniform trend. The two steps at 2325 K and 1809 K are above calculations, the amounts of Fe added to the reaction were between 0 and 60 wt.%. 60% of theoretical density was prepared associated with the melting of alumina and iron, respectively. According to thermodynamic calculations, if the iron added to the reaction is lower than 53.14 wt. %, adiabatic temperature is higher than 1800 K and it is expected that the reaction will be volume combusted.

**Table 1: Data of adiabatic temperature (K) function of the iron concentration (wt. %)**

x	T <sub>ad</sub>		Fe weight
0.00	2328	(1)	0.0%
2.30	2328	(2)	27.7%
2.50	2294		29.4%
3.00	2217		33.3%
3.50	2144		36.8%
4.00	2077		40.0%
4.50	2013		42.8%
5.00	1954		45.4%
5.50	1898		47.8%
6.00	1845		50.0%
6.35	1810	(3)	51.4%
7.85	1810	(4)	56.6%
8.00	1797		57.1%
8.50	1762		58.6%
9.00	1727		60.0%

- (1) Melting temperature of alumina; percentage of melted alumina = 99%
- (2) Melting temperature of alumina; percentage of melted alumina = 0%
- (3) Iron melting temperature; percentage of molten iron = 100%
- (4) Iron melting temperature; percentage of molten iron = 0%

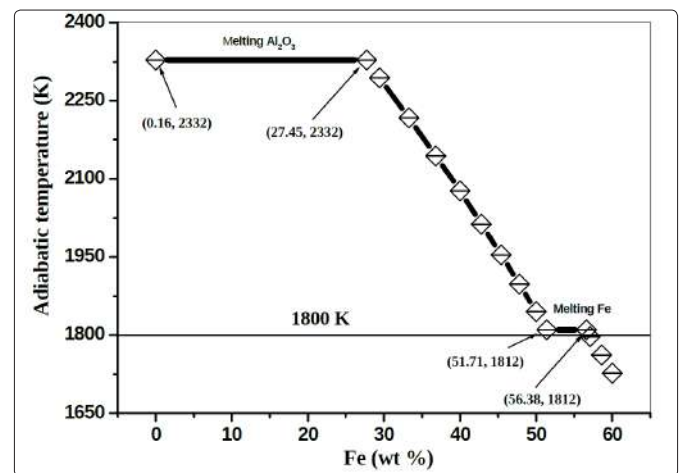


**Figure 2:** Effect of Fe additions on adiabatic temperature of reaction2

The adiabatic temperature for reaction2 with 10 and 20 wt. % Fe is 2325 K which is considerably higher than the Merzhanov criterion (1800 K). This criterion is based on experimental results and it is verified in many ETE-VC in comparison with SHS reaction systems [9]. So, to reveal the reason(s) why it is not applicable for reaction2, phase analysis was performed on the products to investigate the effect of iron addition on phases formed after volume combustion.

The calculation of theoretical adiabatic temperature for this reaction suggests that iron can be added to this reaction up to 56.38 wt. % and it will remain volume combustion according to Merzhanov criterion [9]. But, first experimental investigations showed that in the

sample containing 30 wt.% Fe, the reaction only happened in a thin top surface layer of the compacted powder and then it ended which means that the reaction does not propagate in the ETE-VC mode for this sample. These results are inconsistent with the theoretical results. XRD analysis indicated that the reaction products consist of TiC, Al<sub>2</sub>O<sub>3</sub> and Fe<sub>3</sub>Al intermetallic phases. These reaction products are not the same as the product of reaction2, because in this reaction it was expected that Fe would not participate in the reaction and act only as a diluents agent. But, experimental results showed that some of the aluminum was reacted with iron to form a Fe<sub>3</sub>Al phase. This temperature range is lower than that for ignition of the reaction between aluminum and TiO<sub>2</sub>(1173 K) [14]. So, with the reaction of some of Al with Fe, there will be lack of aluminum for complete reduction of all the TiO<sub>2</sub> to Ti. Choi and Rhee [14] indicated that reduction of TiO<sub>2</sub> with aluminum proceeds by way of Ti<sub>3</sub>O<sub>5</sub>, Ti<sub>2</sub>O<sub>3</sub>.

### XRD analysis

XRD analysis of the samples which contains 20 to 40 wt. % Fe is demonstrated in Fig. 3. The only phases formed in the sample with no Fe are titanium carbide (TiC, ICDD card no. 00-003- 1213) with a cubic crystal structure and aluminum oxide ( $\alpha$ -Al<sub>2</sub>O<sub>3</sub>, ICDD card no. 01-071-1126) with rhombohedral (hexagonal) crystal structure. The addition of 10 wt.% Fe had no considerable effect on XRD pattern, but in samples containing 20 and 40 wt.% Fe, the only phase added to the products was iron aluminide (Fe<sub>3</sub>Al, ICDD card no. 00-045-1203) with a cubic crystal structure. So, reaction products formed in the reactions containing Fe were not as the same as predicted by reaction2. The lattice parameter of titanium carbide was calculated from the XRD patterns using Brag's equation and Nelson–Riley function [3,22].

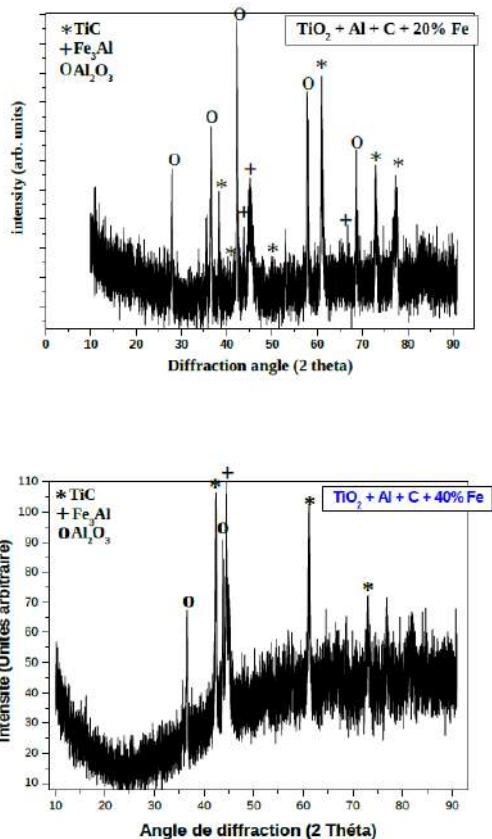


Figure 3: XRD analysis of samples with 20 and 40 wt.% Fe

$$a = a_0 + a_0 K_r \frac{1}{2} \left( \frac{\cos^2 \theta}{\sin \theta} + \frac{\cos^2 \theta}{\theta} \right) = a_0 + K''(\theta)$$

Nelson–Rileyfunction (7)

$a = d(hkl) [h^2 + k^2 + l^2]^{1/2}$  Bragequation (8)

Where  $\theta$  is diffraction angle, is the lattice parameter which is determined by Eq.(7) and  $a_0$  is the true lattice parameter of TiC which is calculated by Eq.(6). Using XRD patterns, we can draw the variations of lattice parameter versus Nelson–Riley function and extrapolate the true lattice parameter at  $\theta=90$ . Fig. 4a and b shows Nelson–Riley function diagrams used for calculating lattice parameter of TiC in samples containing 20 and 40 wt. % Fe and variations of synthesized TiC lattice parameters with iron addition, respectively. Also, the lattice parameter of stoichiometric Ti<sub>0.5</sub>C<sub>0.5</sub> is indicated in the figure.

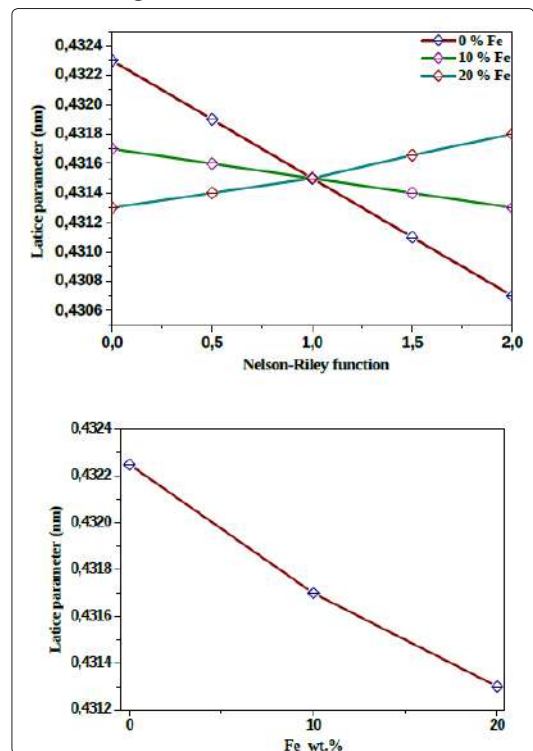


Figure 4: a: Nelson–Riley function diagram for samples with different Fe contents and b: variations of TiC lattice parameter with Fe additions

As can be understood, the lattice parameter of titanium carbide in the sample synthesized without Fe is lower than that of the stoichiometric one and decreases with the increase of Fe content in the reaction.

Different literature that used SHS for synthesis of TiC and composites containing this compound showed that during combustion synthesis, carbon content in the TiC is usually lower than stoichiometric and therefore its formulation represented as TiC<sub>1-x</sub> ( $x \leq 1$ ) [3,23,24]. Storms indicated that by decreasing carbon content, lattice parameter of TiC falls [24]. So, a possible reason for lower lattice parameter of TiC in the sample with higher Fe may be decreasing carbon

of this phase. Another reason for this phenomenon may be the dissolution of oxygen in the crystal structure of TiC and formation of titanium oxy-carbide. Titanium carbide (TiC) has a NaCl face centered cubic (FCC) crystal structure. TiO also has the same crystal structure of TiC. So, they can form a series of continuous solid solutions like  $\text{TiC}_{1-x}\text{O}_x$  ( $0 \leq x \leq 1$ ). Titanium oxy-carbide ( $\text{TiC}_{1-x}\text{O}_x$ ) is an intermediate product usually observed during carbothermal reduction of  $\text{TiO}_2$ . Jiang et al. showed that as TiO increases in the titanium oxy-carbide phase, lattice parameter of this phase falls from 0.4324 nm for TiC to 0.4194 for TiO [25]. and TiO mid-products to form Ti and  $\text{Al}_2\text{O}_3$ . Similar results were presented by Khoshhal and co-workers and Zou et al. [20,26] during aluminothermic reduction of ilmenite. Because there was not any peak related to the  $\text{TiO}_2$  in the XRD patterns and the characteristic peaks of this phase in the Raman spectra were weak, so it is expected that the quantity of this phase is low in all samples. Therefore, the lack of aluminum for complete reduction of  $\text{TiO}_2$  caused partial reduction of it and formation of lower titanium oxide like  $\text{Ti}_3\text{O}_5$ ,  $\text{Ti}_2\text{O}_3$  and TiO and  $\text{Al}_2\text{O}_3$ . Then these oxides reacted with carbon to form oxy-carbide ( $\text{TiC}_{1-x}\text{O}_x$ ) as indicated by XRD analysis through decreasing of lattice parameter of TiC and characteristic peaks of this phase in Raman spectroscopy results. Comparing the lattice parameter calculated for Ti(C,O) in the sample containing 20 wt.% Fe with that proposed by Jiang et al., it is anticipated that the maximum oxygen content of titanium oxy-carbide (x) will be 0.3 and so the chemical formula of the oxy-carbide is  $\text{TiC}_{0.7}\text{O}_{0.3}$  in this sample [25]. The presence of  $\text{TiO}_2$  peaks in the Raman spectra of samples containing 10 and 20 wt.% Fe may be because of this fact that raw materials were not uniform and adding Fe to them raised the distance between  $\text{TiO}_2$  and Al particles. So, in some places of the compacts, Al and  $\text{TiO}_2$  might not be in contact together and therefore no reduction happened. In reaction 2, it was expected that all the carbon reacts with Ti to form stoichiometric titanium carbide. But, Raman analysis of the sample with no Fe showed characteristic peaks of un-reacted carbon. In other words, it indicated that in the aluminothermic reduction of  $\text{TiO}_2$ , all the carbon did not react with the titanium. So, the titanium carbide formed would not be a stoichiometric one and its chemical formula is  $\text{TiC}_x$  ( $x \leq 1$ ). This result is in agreement with the difference observed in Fig. 6 between the lattice parameters of the stoichiometric TiC and that measured for synthesized TiC in the sample with no Fe. When the amount of Fe added to the reaction increased, more aluminum was used in the reaction with Fe, so the volume fraction of reduced Ti falls. As a result, the quantity of titanium oxide mid products and the possibility for the formation of titanium oxy-carbide with higher oxygen content and lower lattice parameter increased as shown in Fig. 6. Also, the increase of oxygen in the titanium oxide mid-product and the decrease of combustion temperature with the addition of Fe reduced the amount of carbon participated in the reaction and led to the increase in volume fraction of un-reacted carbon in the final products as indicated by the amplification of carbon peaks in the Raman spectra of samples with higher Fe

contents (Fig. 7d). It should be noted that the possibility of reducing the remaining  $\text{TiO}_2$  with excess carbon (carbothermal reaction) in the samples containing Fe is low due to the two following reasons: first, according to thermodynamic data, the standard Gibbs free energy of the reaction between  $\text{TiO}_2$  and carbon is positive below 1473 K and therefore this reaction proceeds at very high temperatures (1973–2373 K) in argon atmosphere [22]. As indicated in Fig. 1, the adiabatic temperature of the aluminothermic reaction is 2371 K and adding Fe to the reaction decreased it considerably. Usually, the combustion temperature of an ETE-VC reaction is lower than the adiabatic temperature due to the heat loss to the surrounding area [8,9,16]. So, it is expected that as the Fe was added to the reaction, the combustion temperature decreased which lowered the possibility of carbothermal reaction. Second, carbothermal reduction of  $\text{TiO}_2$  needs high reaction times (10–24 h) [22]. But, the reaction times for small SHS samples are in the range of seconds to a few minutes. So, one can expect that although this reaction can happen during SHS of the present samples, especially in the samples with lower Fe contents due to their higher combustion temperature, but, the extent of its propagation was not high and therefore the amount of carbon used for carbothermal reduction of  $\text{TiO}_2$  was negligible. According to the above Results and Discussion sections, it is expected that the right pass for reaction2 will be as follows: Fig. 9 shows the effect of Fe on adiabatic temperature of reaction 6 which was estimated using the thermodynamic data of Table 1 with this assumption that at low oxygen content, the thermodynamic properties of titanium oxy-carbide ( $\text{TiC}_{1-x}\text{O}_x$ ) are the same as those of titanium carbide (TiC). The effect of Fe on adiabatic temperature of reaction2 is also shown on the figure for comparison. It is observed that the adiabatic temperatures of reaction 6 were 1916 and 1421 K for the samples containing 15 and 20 wt. % Fe which are respectively higher and lower than Merzhanov criterion. So, these new calculated values are consistent with the Merzhanov criterion and experimental observations shown in Fig. 4. As shown earlier in Fig. 4, the reaction is stable for the sample containing 15 wt% Fe, but, not stable for the sample containing 20 wt. % Fe. So, the Merzhanov criterion is satisfied between these two values as indicated in Fig. 9. It is worse noting that if 20 wt. % Fe is added to reaction6, the amount of oxygen (x) in theta ( $\text{C}_{1-x}\text{O}_x$ ) phase will be 0.29. This result is in agreement with the lattice parameter of titanium oxy-carbide purposed by Jiang and that was calculated in Fig.6 [25].

### Microstructural analysis

The FESEM microstructures of the surfaces of samples are illustrated in Fig. 5. Indicate the presence of higher density in the final structure of the products [9]. The microstructure of the sample with no Fe consists of large  $\text{Al}_2\text{O}_3$  grains and TiC particle sintered together (Fig. 5a). The addition of 10 wt. % Fe to the reaction changed the morphology of  $\text{Al}_2\text{O}_3$  from the large platelike grains to slightly finer grains with near spherical morphology. Also, TiC grain size decreased and they became almost spherical in this sample (Fig. 5b).

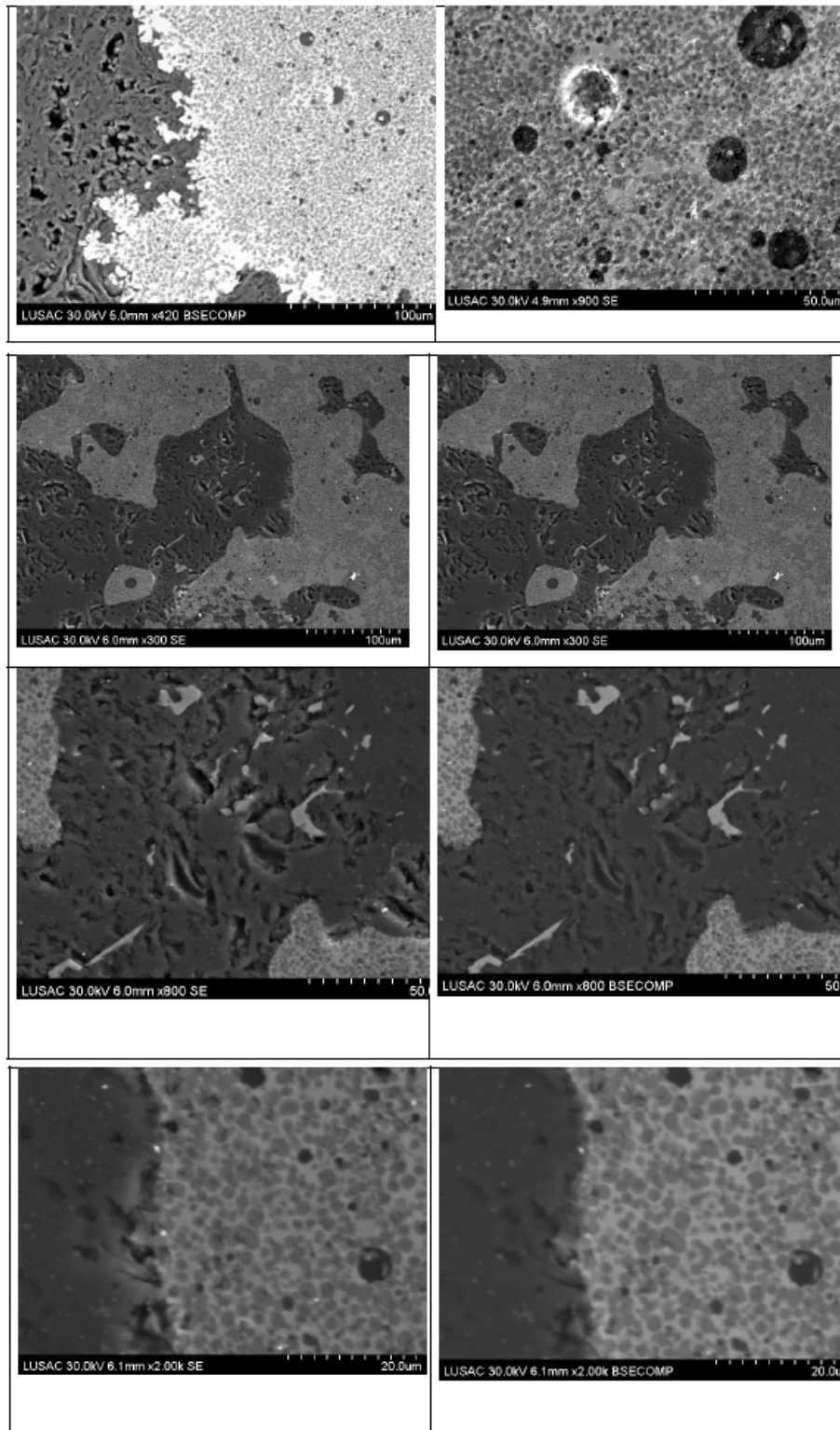


**Figure 5a:** FESEM microstructures of polished and etched surface of samples with 10 wt.% Fe

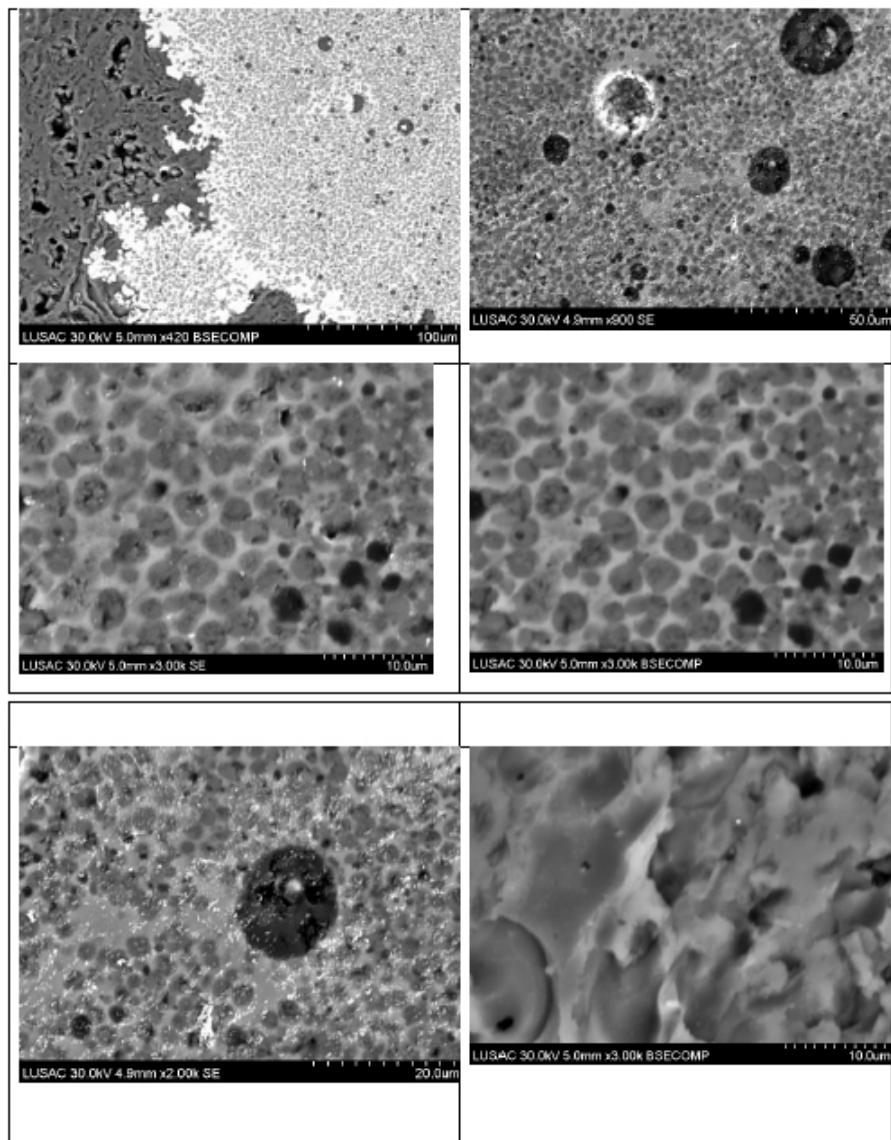


**Figure 5b:** FESEM microstructures of polished and etched surface of samples with 20 wt.% Fe

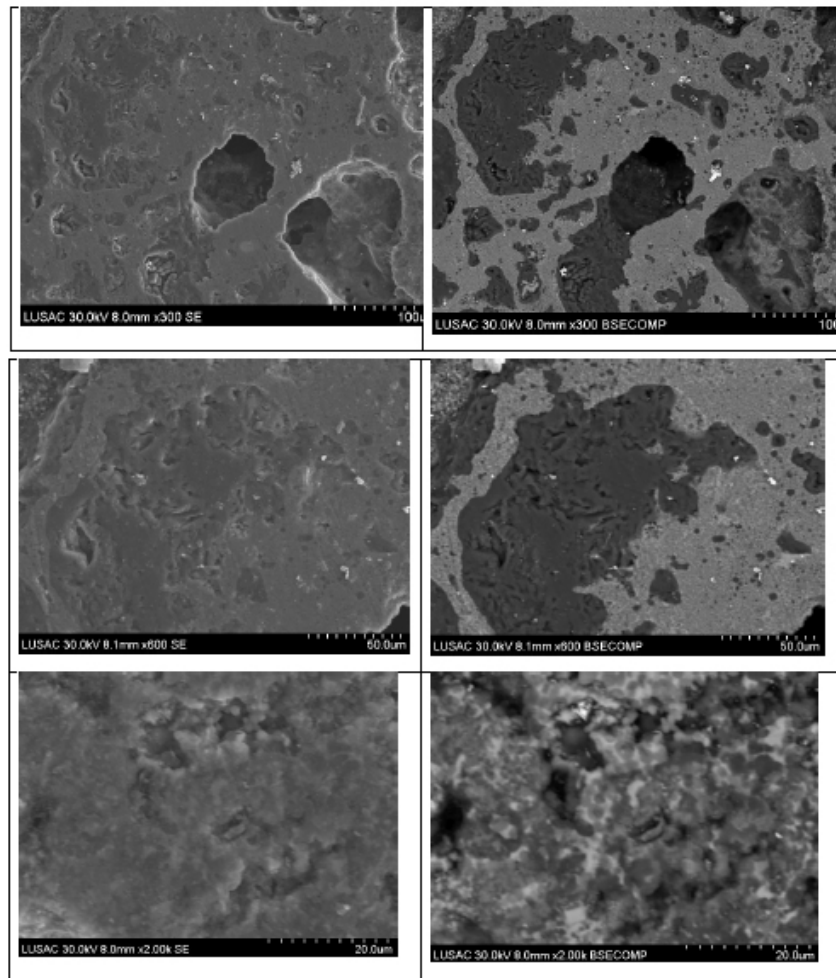


**Figure 5c:** FESEM microstructures of polished and etched surface of samples with 40 wt.% Fe

In the sample containing 20 wt. % Fe, the TiC particles became finer, with a particle size between 2 and 6  $\mu\text{m}$ ), activated carbon (Merck, 102184), fine aluminum powder (Rankem, A2265) and ironm (Fig. 5c and d). It is interesting to notice that there are repeating step on some surfaces of the TiC particles. These steps are characteristics of crystal growth with interface- controlled growth mechanism. Usually, crystal growth in the vapor phase or melt is controlled by three different mechanisms, including diffusion in the melt or vapor, latent heat flow from the crystal-melt interface and reaction at the crystal interface or interface-controlled continuous and lateral growth [27]. The interface-controlled growth mechanism is divided into two different categories named.

In continuous growth, atoms can attach to the crystal surface at any point of the growing surface. In these conditions the interface grows uniformly. But, lateral growth leads to the movement of a step across the interface and the atoms only can attach to the step. The step height can be one, several or a great number of atom layers (macro steps) depending on its lateral growth rate and will be higher for a layer with a slower edge growth rate. There are two types of lateral mechanisms, as surface nucleation and screw dislocation. In surface nucleation mechanism, new steps are nucleated on top of each other and form a pyramid-like interface [28]. On the other hand, the screw dislocation model proposed by Hilling and Turnbull puts on that screw dislocations emerge from the growing crystal face and cause the formation of repeating step like an Archimede an spiral [27,29]. There are some evidences for the formation of two dimensional nuclei on some surfaces of TiC particles. So, it seems that surface nucleation-interface controlled growth mechanism is the growth controlling mechanism of TiC particles in this sample. Fig. 8e and f shows the different magnifications of the fracture surface in the sample containing 20 wt. % Fe. It can be seen that TiC particle size decreased slightly, but their morphology is transformed into cubical particles with faceted morphology. According to the statements of Kirk Patrick faceted, taught there is not a theoretical justification, Cahn et al [27]. suggested that crystals with non-faceted morphology grow by continuous mechanism while crystals with faceted morphology, grow with lateral growth mechanism. Choi and Rhee suggested that the alumino thermic reduction of  $\text{TiO}_2$  is controlled by the diffusion of carbon through solid TiC[14]. So, it seems that the addition of Fe to the reaction changed the mechanism controlling the growth of TiC particles from diffusion controlled growth in the sample without Fe to lateral growth interface controlled mechanism for samples containing Fe higher than 10 wt.%. The addition of higher Fe to the reaction caused the decrease of TiC particle size and porosity volume fraction in this sample.



In the Fig.6, the microstructural representation and EDS analysis displays elemental analyses of the various regions of the samples. Secondary electron image, atomic concentration cartographies of Ti, C, Al and C are also illustrated. EDS spectra and was used to determine the elemental composition of the different regions in the sample with Fe addition and are presented at the Fig. 7.

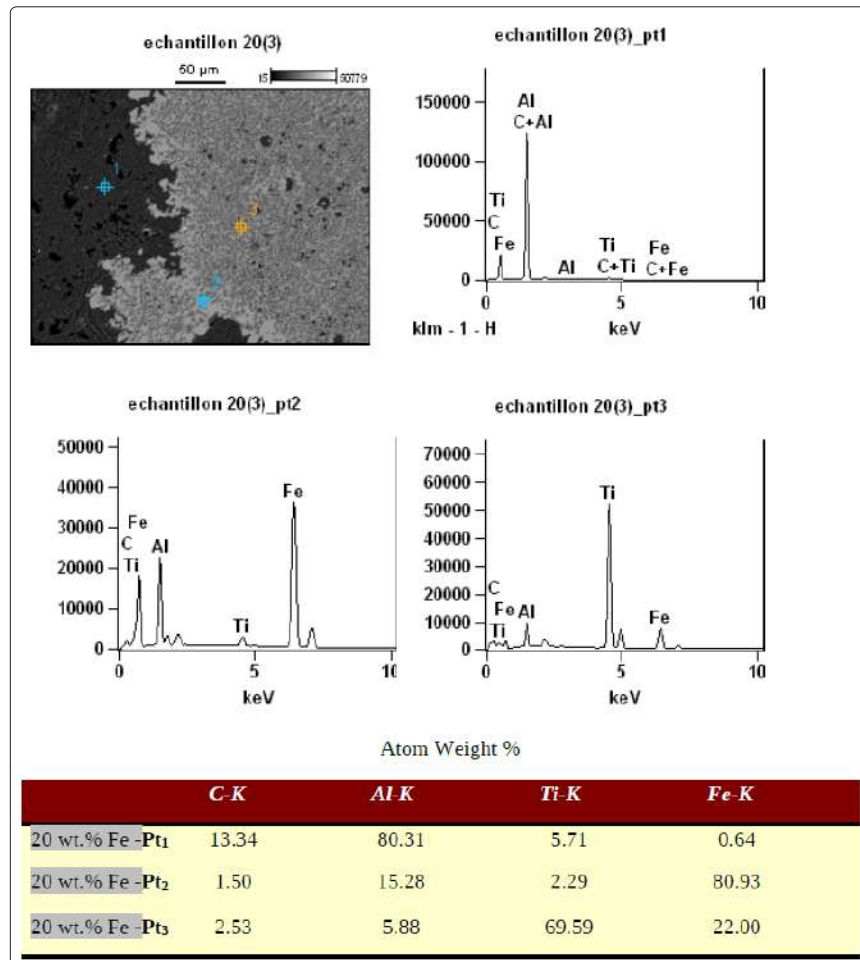


**Figure 6:** EDX spectra in differents region of the high performance composite of polished and etched surface

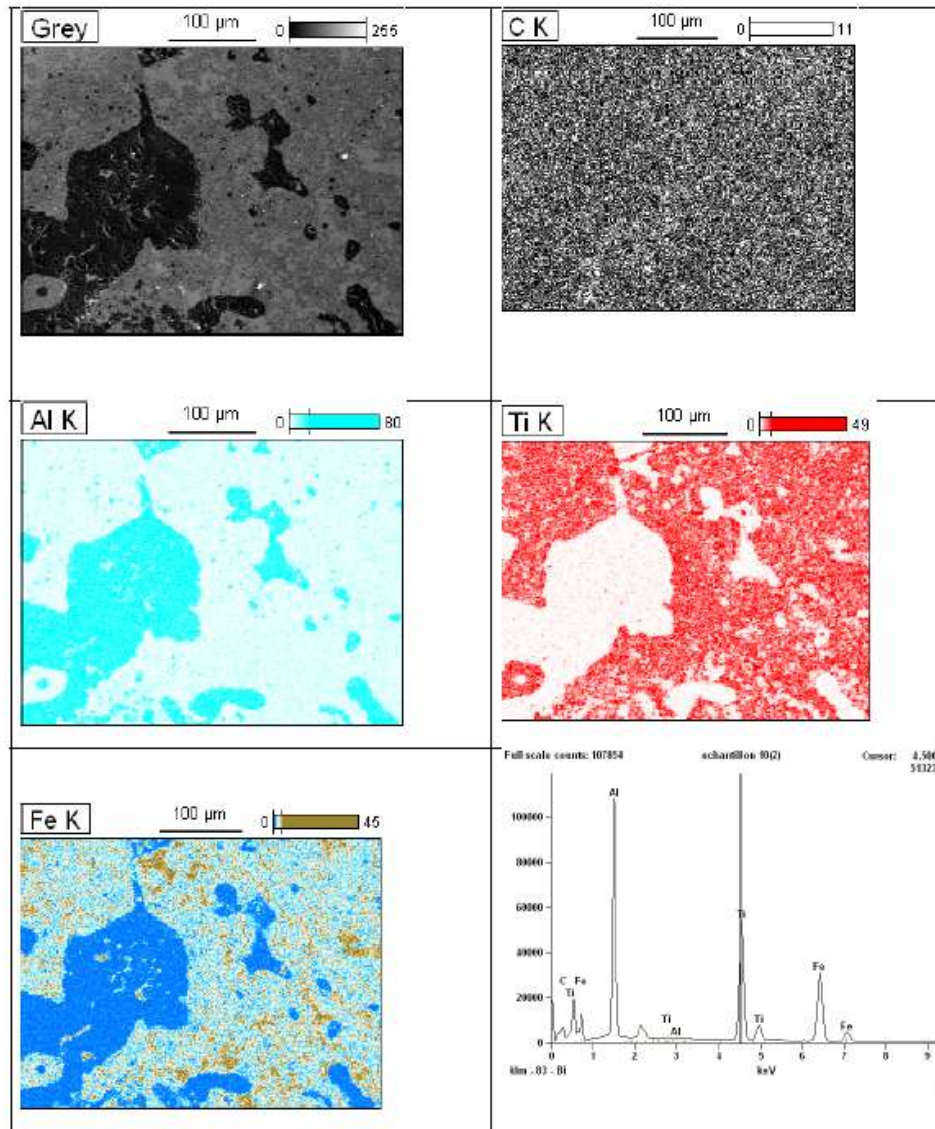


**Figure 7:** Microstructural representation of produced samples, analysis displays elemental analyses of the various regions of the sintered samples. Secondary electron image, atomic concentration cartographies of Fe, Ti, Al and C of polished and etched surface

### Raman analysis

Raman microscopy is able to determine phases for polymorphic solids at the microscopic level. This is its advantage over conventional X-ray diffraction spectrometry in which the sample volume cannot be too small. Phase identification with Raman spectroscopy uses the characteristic vibration band(s) associated with a certain phase in a solid. This analysis is founded on the Raman scattering of electromagnetic radiation by atoms and molecules. When irradiating materials with electromagnetic radiation of a single frequency, the light will be scattered by molecules elastically and inelastically. The inelastic scattering is called Raman scattering and can be used to determine details of the structure of the molecule or crystal lattice [30].

To study the reaction products more precisely, micro-Raman spectroscopy analysis was performed on different samples. Some Raman spectroscopy analysis on titanium carbide reported that the stoichiometric titanium carbide has no Raman active mode and the Raman scattering in this carbide is caused by the disorder induced by carbon vacancy [31,32]. Fig. 8 shows the results of the Raman spectroscopy analysis in the samples containing 0, 10 and 20 wt. % Fe, respectively. In the sample without Fe, five different peaks can be observed (Fig. 8a). The first three peaks between 244 and 255, 414 and 422 and 598 and 601  $\text{cm}^{-1}$  are related to the titanium carbide, which is almost the same as those reported by Lohse et al. and the two peaks between 1300 and 1600 are related to the unreacted free active carbon (Fig.8b) [33].

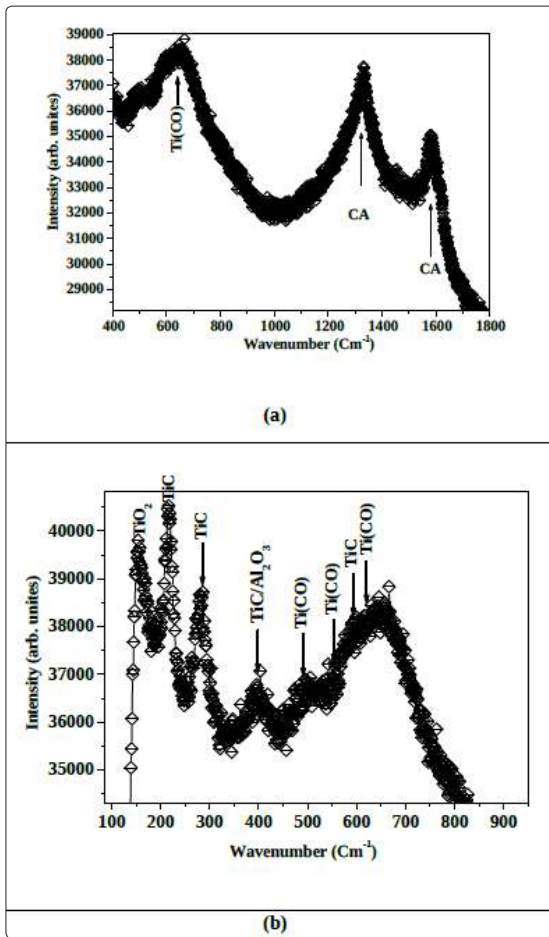


**Figure 8:** Raman spectroscopy analysis of samples with 20 wt.% Fe and d: Raman spectra of TiC and Carbon active in samples with different Fe contents.

There is no separate characteristic peak related to  $\text{Al}_2\text{O}_3$ . Cava et al. reported that  $\text{Al}_2\text{O}_3$  with a cubic crystal structure has no Raman active mode while  $\alpha\text{-Al}_2\text{O}_3$  with a hexagonal crystal structure has two Raman active modes with characteristic peaks at 380 and 420  $\text{cm}^{-1}$  [33]. As shown by XRD analysis, the synthesized alumina in all samples has a hexagonal crystal structure and thus should have two characteristic peaks. But, it seems that these peaks have overlapped with intense TiC characteristic peak at 420  $\text{cm}^{-1}$  and could not be observed in these spectra. The addition of 10 wt. % Fe to the reaction led to the formation of a new peak at 266, some peaks between 340 and 384  $\text{cm}^{-1}$  and two new peaks at 517 and 634  $\text{cm}^{-1}$ . Also, there is a broad peak between 278 and 351  $\text{cm}^{-1}$ , a new peak at 649  $\text{cm}^{-1}$  and a broad peak between 680 and 950  $\text{cm}^{-1}$  in the sample containing 20 wt.% Fe. By comparing the results of this table with the Raman spectra in Fig. 8a, it can be concluded that besides TiC and un-reacted carbon, there is a little  $\text{TiO}_2$  with two weak characteristic peaks at 517 and 634–649  $\text{cm}^{-1}$ . Also, some peaks between 266 and 384  $\text{cm}^{-1}$  and two broad peaks between 550 and 620  $\text{cm}^{-1}$  and 680 and 950  $\text{cm}^{-1}$  are symptoms related to the formation of titanium oxy-carbide ( $\text{Ti}(\text{C},\text{O})$ ) in the final products [34–37]. Getting hold of the results of XRD and Raman together, it can be

concluded that the addition of Fe to reaction 2 led to the increase of oxygen content in the crystal structure of TiC and formation of titanium oxy-carbide with lower latticeparameter.

In Raman spectroscopy, the intensity of phase characteristic peaks is dependent on its quantity. Fig. 8a compares the mean spectrum of the free carbon in the samples synthesized with different Fe contents. It can be seen that the addition of Fe to the reaction increased the mean intensity and surface area of un-reacted carbon characteristic peaks. So, one can anticipate that the volume fraction of unreacted carbon is higher in the sample with more Fe content.

### Vickers microhardness and fracture toughness ( $K_{IC}$ )

According to the above results, it can be concluded that the Vickers hardness has been improved by adding % Fe and enhanced with the fracture toughness value giving a better ductility for thereinforced **high performance ceramic matrix composite** samples. Fig. 9 shows the hardness as a function of the applied indentation load for the same sample. The Vickers hardness increases with the increasing of the wt% of Fe addition. At lower loads, the microhardness reaches a low hardness a constant value of 47.55 GPa at 40 wt% of Fe at  $\text{HV}_{50}$  of the high performance ceramics matrixcomposites [38–40].

Fig. 9 present the variation of Vickers microhardness of the product of reaction 2 with and without Fe addition up to 40 wt. Fe **high performance ceramic matrix composite** with the indentation lead. The microhardness of the composites increased almost linearly with Fe addition. The hardness of **Carbon (28–30 GPa)** is nearly 2 times the previously reported values of hardness of **TiC (18 GPa)**. For the nearly single phase  $\text{Al}_2\text{O}_3$  in this investigation, the microhardness was found to be 8 GPa (measured with indentation load of 300 N), which is higher than the previously reported hardness values for hexagonal in the literature. The microhardness of  $\text{Fe}_3\text{Al}$  is 9.8 GPa While the higher microhardness of the  $\text{TiC-Al}_2\text{O}_3\text{-Fe}_3\text{Al-C}$  composite ceramic matrix is at higher wt. % Fe addition.

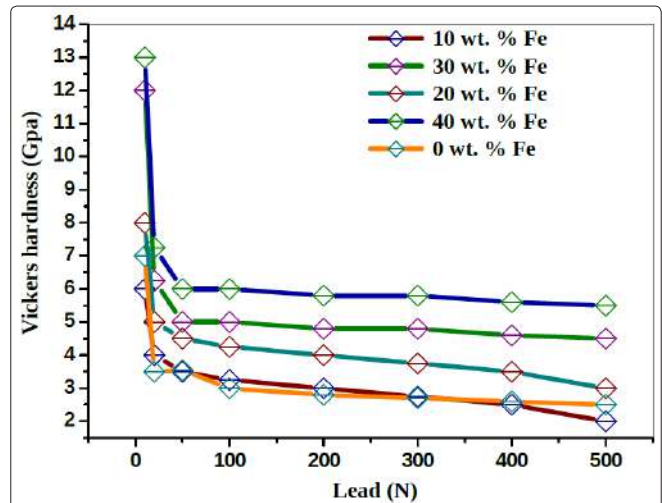
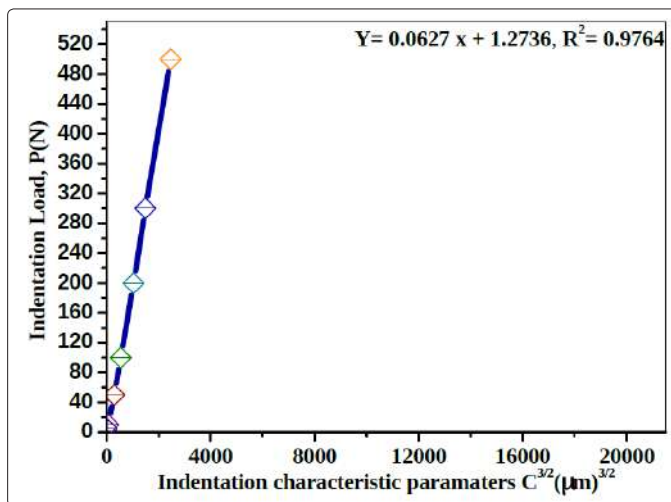


**Figure 9:** Representation the variation of Vickers microhardness function of the indentation leads of the sintered samples using a 20-mm

The highest Vickers microhardness in the range of about 15 GPa was found for lower loads (10 N). A slight increase in average microhardness have been obtained from composites prepared by volume combustion reaction exhibited highest hardness of about 6.50 GPa was found for higher loads (500 N) at higher Fe addition. 40 wt. %.

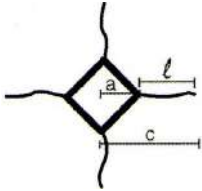
The relevant data were listed in Table 2. In Fig. 10, a linear regression analysis was applied to the relations of P and  $c^{3/2}$  by the least square method.

As a result, the calculated slope A and intercept B were 0.0627 and 1.2736, respectively. The indentation fracture toughness was calculated to be 4.30 MPa  $m^{1/2}$  for 40 wt. % Fe addition ceramics matrix composite (CMCs) with excellent wear resistant will be confirmed [21,41,42].



**Figure 10:** Correlation in between the applied load P and half-length of median crack  $c^{3/2}$  of polished and etched surface for the sintered samples using the (IF) method.

**Table 2: Data of Vickers indentation cracks and fracture toughness (KIC)**

Sintred samples	Half-length of indentation diagonal a (μm)	l (μm)	Half length of median crack c(μm)	Indentation parameter $c^{3/2}$ (μm) <sup>3/2</sup>	KIC (Gpa m <sup>1/2</sup> )	HV (GPa)	
20 wt. % Fe 	P=500 N, Hv50	152.2	467.8	500	122309.74	4.55	3.98
	P= 300 N, Hv30	170.1	450.3	352.3	58007.62	4.59	4.10
40 wt. % Fe	P=500 N, Hv50	95.1	227	191.1	1243019.54	4.70	5.50
	P= 300 N, Hv30	90.23.5	324	356.5	59107.62	4.90	6.12
0 wt. % Fe	P=500 N, Hv50	73.2	157.7	220.9	152309.66	3.65	3.00
	P= 300 N, Hv30	85.29	146.3	165.6	60009.97	3.75	3.50

The addition of Fe plays a important role in sintering additive (the ductility) in the propagation of failer in this nanocomposites and thus enhance the fracture toughness in comparasion with his higher hardness In addition, a high determination coefficient ( $R^2$ ) of 0.9764 was obtained through the linear regression model. IF (indentation fracture) was shown to be an effective method in the evaluation of fracture toughness for its convenience and material saving.

## Conclusions

In the present research, several quantities of Fe were added to the ETE-VC reaction of the TiO<sub>2</sub>-Al-C system to fabricate Fe-TiC-Al<sub>2</sub>O<sub>3</sub> high performance composite ceramic matrix. The main results can be summarized as follows:

1. Thermodynamic calculations predict that if the amount of Fe is lower than 53.13 wt. %, the reaction ignition and volume combustion mode processed.
2. Phase analysis using XRD and Raman spectroscopy indicated that Fe<sub>3</sub>Al, Ti(C, O) and Al<sub>2</sub>O<sub>3</sub> in addition TiB<sub>2</sub> with some residual un-reacted carbon were the main products of the synthesis in the samples containing wt. % Fe. These products were not the same as those expected earlier.
3. Using Raman spectroscopy analysis, it was demonstrated that all the carbon did not react with Ti in the sample containing no Fe and therefore the C/Ti ratio in the TiC phase was less than unity. This led to a lower lattice parameter for the synthesized TiC in comparison to stoichiometric one. Also, the lattice parameter of Ti (C, O) phase was lower in the samples containing higher Fe, likely as a result of dissolution of higher oxygen in this phase.
4. Microstructural observations showed that additions of Fe changed the growth controlling mechanism of TiC particles.
5. The adiabatic temperatures calculated using the thermodynamic data of the new products function of 10 to 40wt. % Fe content were in conformance with the Merzhanov criterion.

## Acknowledgements

We are grateful to **Aurélien Lepeutrec** and **Ibrahim Itaait** (LUSAC, EA 4253, Université de Caen Basse-Normandie (UCBN), **Cherbourg-Octeville**, France) for the helps in the FESEM.

## References

1. Zhu H, Dong K, Wang H, Huang J, Li J, et al. (2013) Reaction mechanisms of the TiC-Fe composite fabricated by exothermic dispersion from Fe-Ti-C element system. *Powder Technol* 246:456-461.
2. Wang XH, Zhang M, Zou ZD, Song SL, Han F, et al. (2006) In situ production of Fe-TiC surface composite coatings by tungsten-inert gas heat source. *Surf Coat Technol* 200: 6117-6122.
3. Razavi M, Rajabi-Zamani AH, Rahimpour MR, Kaboli R, Ostad Shabani M, et al. (2011) Synthesis of Fe-TiC-Al<sub>2</sub>O<sub>3</sub> hybrid nanocomposite via carbothermal reduction enhanced by mechanical activation. *Ceram Int* 37: 443-449.
4. Zhang W, Zhang X, Wang J, Hong C (2004) Effect of Fe on the phases and microstructure of TiC- Fe cermets by combustion synthesis/quasi-isostatic pressing. *Mater Sci Eng A* 381: 924.
5. Bendjemil B, Zemmour K, Gunth A, Leonhardt A, Langlois P, et al. "Study on the Synthesis and Structural Characterization of the Cermets TiC/Fe by Self-Propagating-High- Temperature Synthesis and by Thermal Explosion" *Inter. Journal of SHS* 1: 85.
6. Fatemi Nayeri SHR, Vahdati Khaki J, Aboutalebi MR (2009) Implementation of combined mechanical activation and thermal analysis for identification of combustion synthesis mechanism in TiO<sub>2</sub>-Al-C system. *Iran J Mater Sci Eng* 6: 7-14.
7. Fatemi Nayeri SHR, Vahdati Khaki J, Aboutalebi MR (2006) The effect of milling conditions on the mechanical alloying and combustion synthesis of TiO<sub>2</sub>-Al-C powder mixture. *Iran J Mater Sci Eng* 3: 25-31. Sharifitabar M (2014) *Int. Journal of Refractory Metals and Hard Materials* 47: 93-101
8. Zou B, Xu J, Wang Y, Zhao S, Fan X, et al. (2013) Self-propagating high-temperature synthesis of TiC-TiB<sub>2</sub>-based Co cermets from a Co-Ti-B<sub>4</sub>C system and fabrication of coatings using the cermet powders. *Chem Eng J* 233: 138-148.
9. Moore JJ, Feng HJ (1995) Combustion synthesis of advanced materials: part I. Reaction parameters. *Prog Mater Sci* 39: 243-273.
10. Lee JH, Ko SK, Won CW (2001) Combustion characteristics of TiO<sub>2</sub>-Al-C system. *Mater Res Bull* 36: 1157-1167.
11. Amel-Farzad H, Vahdati-Khaki J, Haerian A, Youssefi A (2008) Combustion wave stability in diluted TiO<sub>2</sub>/Al/C system in atmospheric air. *Solid State Sci* 10: 1958-1969.
12. Xia TD, Munir ZA, Tang YL, Zhao WJ, Wang TM (2000) Structure formation in the combustion synthesis of Al<sub>2</sub>O<sub>3</sub>-TiC composites. *J Am Ceram Soc* 83: 507-512.
13. Bowen CR, Derby B (1996) The formation of TiC-Al<sub>2</sub>O<sub>3</sub> microstructures by a selfpropagating high-temperature synthesis reaction. *J Mater Sci* 31: 3791-3803.
14. Choi Y, Rhee SW (1995) Reaction of TiO<sub>2</sub>-Al-C in the combustion of TiC-Al<sub>2</sub>O<sub>3</sub> composite. *J Am Ceram Soc* 78: 986-92.
15. Saidi A, Chrysanthou A, Wood JV, Kellie JLF (1994) Characteristics of the combustion synthesis of TiC and Fe-TiC composites. *J Mater Sci* 29: 4993-4998.
16. Saidi A, Chrysanthou A, Wood JV, Kellie JLF (1997) Preparation of Fe-TiC composites by the thermal-explosion mode of combustion synthesis. *Ceram Int* 23: 185-189.
17. Cho CH, Kim DK (2002) Microstructure evolution and isothermal compaction in TiO<sub>2</sub>-Al-C combustion reaction. *J Mater Synth Process* 10: 127-134.
18. Xia TD, Liu TZ, Zhao WJ, Ma BY, Wang TM (2001) Self-propagating high-temperature synthesis of Al<sub>2</sub>O<sub>3</sub>-TiC-Al composites by aluminothermic reactions. *J Mater Sci* 36: 5581-5584.
19. Zhu H, Jiang Y, Yao Y, Song J, Li J, et al. (2012) Reaction pathways, activation energies and mechanical properties of hybrid composites synthesized in-situ from Al-TiO<sub>2</sub>-C powder mixtures. *Mater Chem Phys* 137: 532-542.
20. Khoshhal R, Soltanieh M, Boutorabi MA (2014) Formation mechanism and synthesis of Fe-TiC- Al<sub>2</sub>O<sub>3</sub> composite by ilmenite, aluminum and graphite. *Int J Refract Met Hard Mater* 45: 53-57.
21. Jianjun Sha, JianLi, Shouhao Wang, Zhaofu Zhang, Yongchang Wang, et al. (2016) *Materials and Design* 107: 520.
22. Sen W, Xu BQ, Yang B, Sun HY, Song JX, Wan HL, et al. (2011) Preparation of TiC powders by carbothermal reduction method in vacuum. *Trans Nonferrous Met Soc China* 21: 185-190.
23. Hajalilou A, Hashim M, Nahavandi M, Ismail I (2014) Mechanochemical carboaluminothermic reduction of rutile to produce TiC-Al<sub>2</sub>O<sub>3</sub> nanocomposite. *Adv Powder Technol* 25: 423-429.
24. Storms EK (1967) *The refractory carbides*. New York: Academic Press.
25. Jiang B, Hou N, Huang S, Zhou G, Hou J, et al. (2013) Structural studies of TiC<sub>1-x</sub>O<sub>x</sub> solid solution by Rietveld refinement and first-principles calculations. *J Solid State Chem* 204:18.
26. Zou Z, Wu Y, Yin C, Li X (2007) Preparation of Fe-Al intermetallic-TiC-Al<sub>2</sub>O<sub>3</sub> ceramic composites from ilmenite by SHS. *J Wuhan Univ Technol Mater Sci Ed* 22: 706-709.
27. Kirkpatrick RJ (1975) Crystal growth from the melt: a review. *Am Mineral* 60: 798-804.

28. Fredriksson H, Akerlind U (2012) Solidification and crystallization processing in metals and alloys. United Kingdom: John Wiley & Sons.
29. Hilling WB, Turnbull D (1956) Theory of crystal growth in pure undercooled liquids. *J Phys Chem* 24: 914.
30. Leng Y (2008) Materials characterization. Singapore: John Wiley & Sons.
31. Klein MV, Holy JA, Williams WS (1978) Raman scattering induced by carbon vacancies in TiCx. *Phys Rev B* 15: 1546-1556.
32. Lohse BH, Calka A, Wexler D (2005) Raman spectroscopy as a tool to study TiC formation during controlled ball milling. *J Appl Phys* 97: 114912-114917.
33. Cava S, Tebcherani SM, Souza IA, Pianaro SA, Paskocimas CA, et al. (2007) Structural characterization of phase transition of Al<sub>2</sub>O<sub>3</sub> nanopowders obtained by polymeric precursor method. *Mater Chem Phys* 103: 394-399.
34. Chakraborty SP, Sharma IG, Suri AK, Bose DK (2001) Studies on preparation, characterization and evaluation of properties of Fe<sub>3</sub>Al-based intermetallic alloy of composition Fe-16Al-5.44Cr-1Nb-0.5C. *J Mater Process Technol* 115: 413-422.
35. Desai PD (1987) Thermodynamic properties of selected binary aluminum alloy systems. *J Phys Chem Ref Data* 16: 109-124.
36. Kubashewski O, Alcock CB (1979) Metallurgical thermochemistry. New York: Pergamon Press.
37. Barin I (1995) Thermochemical data of pure substances. 3rd ed. New York: VCH.
38. Ma J, Yang J, Bi Q, Liu W (2010) Preparation of an ultrafine-grained Fe-40Al intermetallic compound. *Acta Metall Sin* 23: 50-56.
39. Choi HC, Jung YM, Kim SB (2005) Size effects in the Raman spectra of TiO<sub>2</sub> nanoparticles. *Vib Spectrosc* 37: 33-38.
40. Hassan M, Rawat RS, Lee P, Hassan SM, Qayyum A, et al. (2008) Synthesis of nanocrystalline multiphase titanium oxycarbide (TiCxOy) thinfilms by UNU/ICTP and NX2 plasma focus devices. *Appl Phys A* 90: 669-677.
41. Chappé JM, Fernandes AC, Moura C, Alves E, Barradas NP, et al. (2012) Analysis of multifunctional titanium oxycarbide films as a function of oxygen addition. *Surf Coat Technol* 206: 2525-34.
42. Zarezadeh Mehrizi M, Saidi A, Shamanian M, Eslami HR (2011) Combustion synthesis of Fe-Al- TiC composite powders and effect of Al content on its characteristics. *Powder Metall* 54: 400-403.

**Copyright:** ©2019 Badis Bendjemil, et al. This is an open-access article distributed under the terms of the Creative Commons Attribution License, which permits unrestricted use, distribution, and reproduction in any medium, provided the original author and source are credited.